Mon. Not. R. Astron. Soc. **348,** 1401–1408 (2004) doi:10.1111/j.1365-2966.2004.07463.x

Hydrodynamical simulations of the Sunyaev–Zel'dovich effect: cluster scaling relations and X-ray properties

Antonio C. da Silva,[1,2]★ Scott T. Kay,[3] Andrew R. Liddle[3] and Peter A. Thomas[3]

[1]*IAS, Bâtiment 121, Université Paris Sud, F-91405 Orsay, France*
[2]*Observatoire Midi-Pyrénées, Av. Edouard Belin 14, F-31500 Toulouse, France*
[3]*Astronomy Centre, University of Sussex, Falmer, Brighton BN1 9QH*

Accepted 2003 November 20. Received 2003 November 18; in original form 2003 August 13

ABSTRACT

The Sunyaev–Zel'dovich (SZ) effect is a powerful new tool for finding and studying clusters at high redshift, particularly in combination with their X-ray properties. In this paper we quantify the expected scaling relations between these properties using numerical simulations with various models for heating and cooling of the cluster gas. For a *Non-radiative* model, we find scaling relations in good agreement with self-similar predictions: $Y \propto T_{\rm X}^{5/2}$ and $Y \propto L_{\rm X}^{5/4}$. Our main results focus on predictions from *Cooling* and *Preheating* simulations, shown recently by Muanwong et al. to provide a good match to the X-ray scaling relations at $z = 0$. For these runs, we find slopes of approximately $Y \propto T_{\rm X}^{3}$ and $Y \propto L_{\rm X}$, steeper and flatter than the self-similar scalings respectively. We also study the redshift evolution of the scaling relations, and find that the slopes show no evidence of evolution out to redshifts well beyond unity, while the normalizations of relations between the SZ signal and X-ray properties do show evolution relative to that expected from self-similarity, particularly at $z < 1$.

Key words: hydrodynamics – methods: numerical – cosmic microwave background – X-rays: galaxies: clusters.

1 INTRODUCTION

The prospect of surveying for galaxy clusters across a wide range of redshifts using the Sunyaev–Zel'dovich (SZ) effect (Sunyaev & Zel'dovich 1972, 1980) raises the hope of a much-improved understanding of cluster physics, and in particular of the evolution of the cluster gas. The SZ effect is a particularly powerful tool when combined with observations of X-ray emission from the hot cluster gas, as the two techniques probe different properties of the cluster gas distribution. With the *XMM–Newton* and *Chandra* X-ray satellites in their main operations phases, the number of clusters and groups with quality X-ray observations is rapidly increasing. It is therefore timely to extend theoretical models of clusters, where efforts have hitherto been concentrated upon their X-ray properties, to incorporate predictions for the SZ effect.

Numerical simulations indicate that the distribution of non-baryonic dark matter in clusters, which dominates their mass, is approximately self-similar (e.g. Navarro, Frenk & White 1995, 1997). Observations indicate, however, that the baryonic gas component cannot share such a degree of self-similarity. This is particularly evident from observations of the $L_{\rm X}$–$T_{\rm X}$ relation, which show it to be steeper than predicted by the self-similar model (e.g. Edge & Stewart 1991; Xue & Wu 2000). The reason for this discrepancy is that the gas is less centrally concentrated than the dark matter, as a result of physical processes (in addition to gravity) that raised the entropy of the gas (e.g. Evrard & Henry 1991; Kaiser 1991; Bower 1997; Voit et al. 2002; Ponman, Sanderson & Finoguenov 2003). This entropy could come either from direct heating of the hot gas from stars or active galactic nuclei (AGN) (e.g. Wu, Fabian & Nulsen 2000; Bower et al. 2001; Quilis, Bower & Balogh 2001), or from radiative cooling, which transforms low-entropy material into stars, allowing high-entropy material to flow in to replace it (e.g. Knight & Ponman 1997; Pearce et al. 2000; Bryan 2000). Understanding the relative importance of heating and cooling, and how these processes conspire to establish excess entropy in clusters, is one of the key problems in cluster gas physics.

The implications of an excess of entropy on the global properties of the SZ effect (e.g. source counts, mean Compton parameter and angular power spectrum) has previously been investigated using both analytical techniques (e.g. Cavaliere & Menci 2001; Holder & Carlstrom 2001; Zhang & Wu 2003) and numerical simulations (e.g. Springel, White & Hernquist 2001; da Silva et al. 2001; White, Hernquist & Springel 2002). The mass dependence of the SZ effect in clusters has been addressed by Metzler (1998) and White et al. (2002). More recently, McCarthy et al. (2003a) used a semi-analytic model to derive scaling relations between the central Compton parameter and mass, temperature, SZ flux density and X-ray luminosity. These scalings were subsequently used in a companion paper (McCarthy et al. 2003b) to estimate the level of the entropy floor compatible with present-day SZ observations.

★E-mail: antonio.dasilva@ias.u-psud.fr

© 2004 RAS

The purpose of this paper is to investigate the relationship between SZ and X-ray properties of clusters in N-body/hydrodynamical simulations that include models for both cooling and preheating. The simulations we use have already been demonstrated to give good overall agreement with observed X-ray scaling relations at zero redshift (Muanwong et al. 2001, 2002; Thomas et al. 2002). Our approach is mainly focused on the derivation of theoretical scaling laws, and their evolution with redshift, between the integrated SZ flux density and other cluster properties, such as X-ray temperature and luminosity. We quantify deviations from self-similar evolution on both the slope and normalization of the scalings and provide fits that can be used for comparison with other theoretical models and observations. An observationally motivated analysis of SZ/X-ray correlations, which can be more readily applied to 'blind' searches for high-redshift clusters, will be presented in a future paper.

This paper is organized as follows. We define the observational quantities used and the simple scaling laws predicted by the self-similar model in Section 2. Details of our simulations and how our cluster catalogues were constructed are presented in Section 3. In Section 4, we investigate the correlation between thermal SZ integrated flux and other 3D cluster properties (mass, mass-weighted and emission-weighted temperature, and X-ray luminosity) from the simulation data at zero redshift. The evolution of these relations with redshift is studied in Section 5, before we draw conclusions in Section 6.

2 THEORETICAL FRAMEWORK

2.1 Definitions of physical quantities

The SZ effect arises due to inverse Compton scattering of cosmic microwave background (CMB) photons off free electrons, with the largest SZ signal being produced by intracluster gas. The total SZ flux density produced by a cluster is the integral of the SZ sky brightness over its subtended solid angle:

$$S_\nu = I_0 \int [g(x)y - h(x)b]\,\mathrm{d}\Omega, \tag{1}$$

where $I_0 = 2(k_\mathrm{B}T_0)^3/(hc)^2 \simeq 2.28 \times 10^4$ mJy arcmin^{-2},[1] for a mean CMB temperature of $T_0 \simeq 2.725$ K (Mather et al. 1999). The first term inside the square brackets accounts for the thermal SZ effect, due to internal motion of the electrons, whereas the second term, the kinetic SZ effect, is the contribution due to bulk motion of the gas. We ignore the kinetic SZ effect in this paper, because the thermal SZ effect dominates at all frequencies except $\nu \simeq 217$ GHz ($x = h\nu/k_\mathrm{B}T_0 \simeq 3.83$).

The Comptonization parameter y contains information on the structure of the intracluster gas:

$$y = \frac{k_\mathrm{B}\sigma_\mathrm{T}}{m_\mathrm{e}c^2} \int T_\mathrm{e} n_\mathrm{e}\,\mathrm{d}l, \tag{2}$$

where T_e and n_e are the temperature and density of the electrons, $\sigma_\mathrm{T} \simeq 6.65 \times 10^{-25}$ cm^2 is the Thomson cross-section, c is the speed of light and m_e is the electron rest mass. It is therefore convenient to define the integrated contribution to S_ν from y as:

$$Y = \int y\,\mathrm{d}\Omega = \int \frac{y}{d_\mathrm{A}^2}\,\mathrm{d}A = \frac{k_\mathrm{B}\sigma_\mathrm{T}}{m_\mathrm{e}c^2\,d_\mathrm{A}^2} \int_V T_\mathrm{e} n_\mathrm{e}\,\mathrm{d}V, \tag{3}$$

[1] 1 mJy = 10^{-26} erg s^{-1} m^{-2} Hz^{-1}.

where d_A is the angular diameter distance and $\mathrm{d}A = \mathrm{d}\Omega\ \mathrm{d}A^2$ is the sky projected area element of the cluster. Since Y depends on distance, we will usually work with the intrinsic thermal SZ signal, defined as $Y^\mathrm{int} = Y\,d_\mathrm{A}^2(z)$.

The X-ray luminosity of a cluster is

$$L_\mathrm{X} = \int n_\mathrm{e} n_\mathrm{H} \Lambda_\mathrm{c}(T)\,\mathrm{d}V. \tag{4}$$

The integral is over the volume of the cluster and $\Lambda_\mathrm{c}(T)$ denotes the cooling rate of the gas, assuming collisional ionization equilibrium. At temperatures above a few keV, the emission is dominated by thermal bremsstrahlung, but below this line emission becomes important.

2.2 Self-similar scaling relations

In the absence of any non-gravitational heating and cooling processes, clusters scale self-similarly to a good approximation (Kaiser 1986; Navarro et al. 1995). In self-similar models, the temperature of the gas scales with the cluster mass as

$$T \propto M^{2/3}(1+z), \tag{5}$$

assuming the density of the gas scales with the mean density $\rho \propto (1+z)^3$ and the system is in virial equilibrium. Applying this to equation (3) we get

$$Y^\mathrm{int} \propto \begin{cases} f_\mathrm{gas} T^{5/2}(1+z)^{-3/2}, \\ f_\mathrm{gas} M^{5/3}(1+z), \end{cases} \tag{6}$$

where f_gas is the gas mass fraction of the cluster.

The X-ray luminosity of a self-similar cluster scales as

$$L_\mathrm{X} \propto \begin{cases} f_\mathrm{gas}^2 T^2(1+z)^{3/2}, \\ f_\mathrm{gas}^2 M^{4/3}(1+z)^{7/2}, \end{cases} \tag{7}$$

assuming that the X-rays are due to bremsstrahlung emission ($\Lambda_\mathrm{c} \propto T^{1/2}$).

3 METHOD

3.1 Simulation details

Results are presented from three simulations, described in detail elsewhere (Thomas et al. 2002; Muanwong et al. 2002); we summarize pertinent details here.

We assume a ΛCDM cosmology, setting the density parameter $\Omega_\mathrm{m} = 0.35$, cosmological constant $\Omega_\Lambda = 0.65$, Hubble parameter $h = 0.71$, baryon density $\Omega_\mathrm{b}h^2 = 0.019$, CDM power spectrum shape parameter $\Gamma = 0.21$, and normalization $\sigma_8 = 0.9$. These values are similar to those favoured by current observations including *WMAP*. Initial conditions were generated using 160^3 particles each of baryonic and dark matter, perturbed from a regular grid of comoving length $L = 100\ h^{-1}$ Mpc. These choices set the gas and dark matter particle masses equal to $2.6 \times 10^9\ h^{-1}\ \mathrm{M}_\odot$ and $2.1 \times 10^{10}\ h^{-1}\ \mathrm{M}_\odot$ respectively.

The runs were started at redshift $z = 49$ and evolved to $z = 0$ using a parallel version of the HYDRA N-body/hydrodynamics code (Couchman, Thomas & Pearce 1995; Pearce & Couchman 1997), which uses a smoothed particle hydrodynamic (SPH) implementation similar to that discussed in Thacker & Couchman (2000), and conserves both energy and entropy to a satisfactory degree. The gravitational softening was fixed at 50 h^{-1} kpc in comoving coordinates until $z = 1$, then at 25 h^{-1} kpc in physical coordinates until $z = 0$.

The simulations differed only in the adopted heating/cooling model. In the first model, a *Non-radiative* simulation, the gas was subject only to gravitational, adiabatic and viscous forces, and so could only change its entropy through shock heating. This model fails to reproduce the X-ray scaling relations (Muanwong et al. 2001) but nevertheless can be used to test the self-similar scalings presented in the previous section.

The second simulation, a *Cooling* model, allowed gas to cool radiatively as described by Thomas & Couchman (1992). Tabulated values of Λ_c were generated from cooling tables in Sutherland & Dopita (1993), assuming a time-varying global gas metallicity $Z = 0.3(t/t_0)\ Z_\odot$, where $t_0 \simeq 12.8$ Gyr is the current age of the Universe. Cooled material (identified as all gas particles with temperatures $T < 1.2 \times 10^4$ K and overdensities $\delta > 1000$) was converted into collisionless particles. Note that the choice of density threshold (considerably lower than the observed density of star formation) largely circumvents the problem of unphysical cooling of hot gas particles in contact with cold dense gas, as well as increasing runtime efficiency. The global fraction of cooled gas in the simulation box is ~15 per cent at $z = 0$. The removal of this gas from the hot phase sufficiently increases the entropy in the centres of clusters to reproduce the X-ray scaling relations, but the cooled fraction is 2–3 times higher than observed (Cole et al. 2001). In this respect, this run provides a maximum variation of Y from a cluster due to effect of radiative cooling alone.

Finally, the third simulation, a *Preheating* model, also allowed the gas to cool radiatively, but the gas was impulsively heated by 1.5 keV per particle at $z = 4$. This generates the required minimum entropy in the centres of clusters but prevents further cooling to 10^4 K; the global fraction of cooled gas in the simulation box is only ~0.5 per cent at $z = 0$.

Note that we do not attempt to perform a numerical resolution study for this work. Apart from being computationally demanding, it would be misleading to study the effects of resolution on our current models. In particular, increasing the resolution in the *Cooling* model would result in an even higher cooled fraction, and so attaining convergence in this model is undesirable. Instead, we interpret our models as a relatively crude first attempt to capture the effects of increasing the entropy of the gas by the required amount in two completely different ways (i.e. from cooling and heating). A proper convergence analysis is warranted when feedback is included (e.g. Springel & Hernquist 2003) and will be investigated in future work.

3.2 Cluster selection and SZ/X-ray estimators

We identified clusters in our simulations according to the method described in Thomas et al. (1998). Clusters were selected by first creating a minimal spanning tree of all dark matter particles whose density exceeds $\delta = 178\Omega^{-0.55}(z)$ times the mean dark matter density [the approximate value for a virialized sphere, as predicted by the spherical top-hat model (Eke, Navarro & Frenk 1998)]. The tree was then pruned into clumps using a maximum linking length equal to $0.5\delta^{-1/3}$ times the mean interparticle separation. A sphere was then grown around the densest particle in each clump until the enclosed mean density exceeded a value Δ in units of the comoving critical density. For this paper, we use $\Delta = 200$, larger than the virial value for our cosmology ($\Delta \sim 111$) but commonly used by other authors. Master cluster catalogues[2] were produced containing only objects with at least 500 particles each of gas and dark matter, equivalent to a mass limit $M_{\rm lim} \approx 1.18 \times 10^{13}\ h^{-1}\ {\rm M}_\odot$. At $z = 0$, the catalogues contain 428, 457 and 405 clusters for the *Non-radiative, Cooling* and *Preheating* simulations respectively.

For each cluster, we then estimated various observable quantities: the intrinsic SZ signal $Y^{\rm int}$, the X-ray emission-weighted gas temperature $T_{\rm X}$, and the X-ray luminosity $L_{\rm X}$. We identified the hot intracluster gas as all gas particles within R_{200} with $T > 10^5$ K (in practice there are very few particles with 10^4 K $< T < 10^5$ K, as their cooling times are very short) and assume full ionization, such that the number of electrons per baryon is $\eta = 0.88$ for a hydrogen mass fraction $X = 0.76$. We have

$$Y^{\rm int} = \frac{k_{\rm B}\sigma_{\rm T}}{m_{\rm e}c^2}\frac{\eta}{m_{\rm p}} f_{\rm gas} M T_{\rm mw}, \tag{8}$$

where $T_{\rm mw} = \sum m_i T_i / \sum m_i$ is the mass-weighted temperature of the gas, $f_{\rm gas} = \sum m_i / M$ is the gas fraction, m_i is the mass of hot gas particle i and M is the total mass of the cluster.

The X-ray emission-weighted temperature was estimated as

$$T_{\rm X} = \frac{\sum_i m_i \rho_i \Lambda_{\rm soft}(T_i, Z) T_i}{\sum_i m_i \rho_i \Lambda_{\rm soft}(T_i, Z)}, \tag{9}$$

where ρ_i and T_i are the density and temperature of the hot gas particles. Since most observed temperatures use instruments sensitive to soft X-rays, we use a soft-band cooling function, $\Lambda_{\rm soft}$, from Raymond & Smith (1977) for an energy range 0.3–1.5 keV.

The bolometric X-ray luminosity of each cluster, corrected from its soft-band emission, was estimated as

$$L_{\rm X} = \frac{\Lambda_{\rm bol}(T_{\rm X})}{\Lambda_{\rm soft}(T_{\rm X})} \frac{\sum_i m_i \rho_i \Lambda_{\rm soft}(T_i, Z)}{(\mu m_{\rm H})^2}, \tag{10}$$

where $\mu m_{\rm H} = 10^{-24}$ g is the mean molecular mass of the gas and $\Lambda_{\rm bol}$ is the bolometric cooling function (Sutherland & Dopita 1993).

Finally, to avoid introducing artificial trends in the derived scalings with temperature and X-ray luminosity (Sections 4 and 5), we imposed lower limits on $T_{\rm X}$ and $L_{\rm X}$ (by inspecting the $T_{\rm X}$–M and $L_{\rm X}$–M relations at all redshifts) to create (separate) catalogues that were complete in the two quantities. At each redshift, these limits approximately correspond to the maximum temperature and luminosity of all clusters at our mass limit $M_{\rm lim}$. For example, when investigating temperature scalings at $z = 0$, all clusters with $T_{\rm X} <$ 0.35, 0.65 and 0.60 keV for the *Non-radiative, Cooling* and *Preheating* simulations, respectively, were discarded, reducing the number of clusters in our catalogues by around 30 per cent in the *Cooling* and *Preheating* simulations and 46 per cent in the *Non-radiative* run. Similarly, for scalings with X-ray luminosity at $z = 0$, our original cluster catalogues were trimmed by selecting only clusters with $L_{\rm X} > 2.9 \times 10^{43}$, 9.0×10^{41} and 4.5×10^{41} erg s^{-1} for the *Non-radiative, Cooling* and *Preheating* simulations, respectively, reducing the number of clusters in the original catalogues by about 52, 46, and 29 per cent respectively.

4 SCALING RELATIONS AT ZERO REDSHIFT

4.1 The Y–M and Y–$T_{\rm mw}$ relations

We begin by correlating $Y^{\rm int}$ with mass and mass-weighted temperature, all measured within R_{200}. An early study of the relation between mass and SZ absorption in clusters was made in unpublished work by Metzler (1998), who verified with non-radiative simulations the related self-similar scaling, $y \propto M$. More recently, White et al. (2002) also recovered the self-similar scaling, $Y \propto M^{5/3}$, from simulations with the same box size but a slightly higher (factor of 2.5) mass

[2] The catalogues are available to download from the Virgo website, http://virgo.sussex.ac.uk

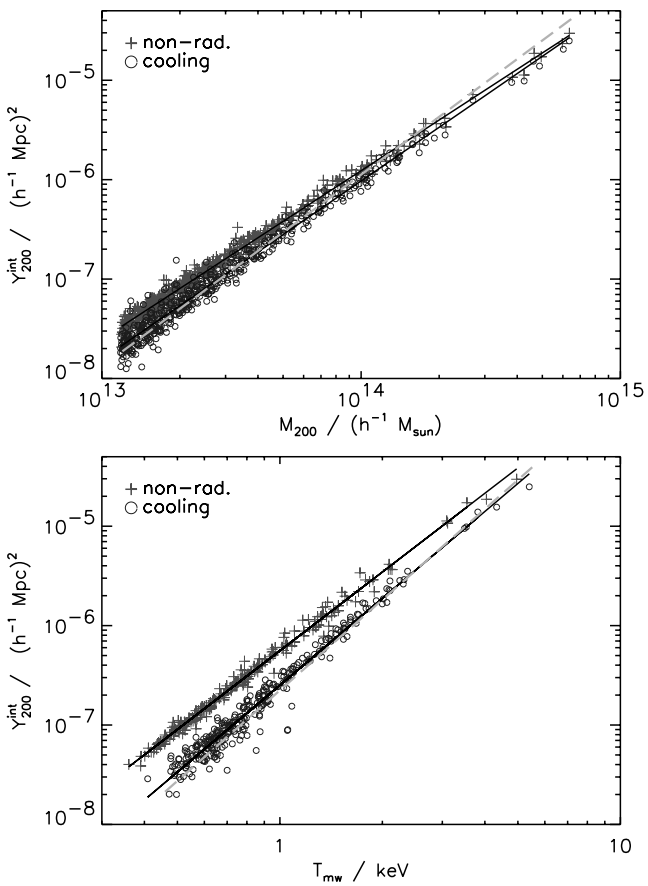

Figure 1. Scaling relations between $Y^{\rm int}_{200}$ and M_{200} (top panel) and $Y^{\rm int}_{200}$ and $T_{\rm mw}$ (bottom panel) for the *Non-radiative* (crosses) and *Cooling* (circles) simulations. Solid lines are power-law fits to the data from these runs, while the dashed line is the corresponding fit for clusters in the *Preheating* simulation.

resolution than that used here, concluding that the combined effect of cooling and feedback (galactic winds) on the SZ properties of their clusters was small.

Fig. 1 illustrates our $Y^{\rm int}_{200}$–M_{200} and Y–$T_{\rm mw}$ relations for clusters in the *Non-radiative* (crosses) and *Cooling* (circles) simulations. The solid lines represent power-law best fits to the data, while the dashed line is the best fit to clusters in the *Preheating* simulation, omitted for the purpose of clarity. The figure shows that $Y^{\rm int}_{200}$ is tightly correlated with mass and mass-weighted temperature in all runs. As we shall see, however, these correlations show significantly less scatter than those relating Y with X-ray emission-weighted properties, because the latter is sensitive to substructure in the dense core gas. The best power-law fits to the $Y^{\rm int}_{200}$–M_{200} relation in each simulation are as follows:

Non-radiative run:

$$Y^{\rm int}_{200} = 1.22 \times 10^{-6} \left(\frac{M_{200}}{10^{14}\, h^{-1}\, {\rm M}_\odot} \right)^{1.69} (h^{-1}\, {\rm Mpc})^2, \qquad (11)$$

Cooling run:

$$Y^{\rm int}_{200} = 0.97 \times 10^{-6} \left(\frac{M_{200}}{10^{14}\, h^{-1}\, {\rm M}_\odot} \right)^{1.79} (h^{-1}\, {\rm Mpc})^2, \qquad (12)$$

Preheating run:

$$Y^{\rm int}_{200} = 1.12 \times 10^{-6} \left(\frac{M_{200}}{10^{14}\, h^{-1}\, {\rm M}_\odot} \right)^{1.93} (h^{-1}\, {\rm Mpc})^2. \qquad (13)$$

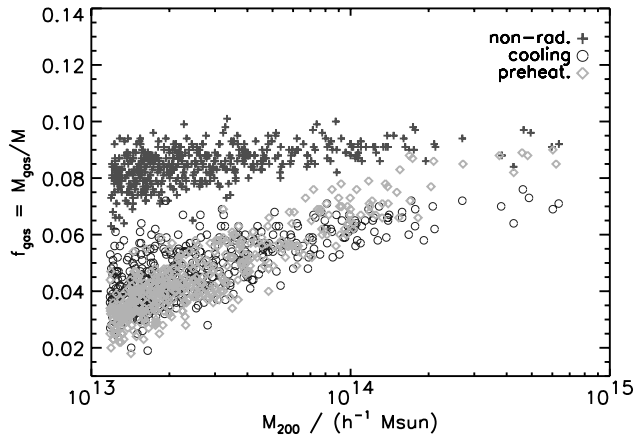

Figure 2. Fraction of hot gas within R_{200} as a function of mass for clusters in the *Non-radiative* (crosses), *Cooling* (circles) and *Preheating* (diamonds) simulations.

As expected, the slope of the fit to the *Non-radiative* clusters is close to 5/3, the self-similar value given in equation (6). The slope is steeper for the *Cooling* and *Preheating* simulations, however, primarily due to lower Y values for low-mass systems. This difference is due to the effects of cooling and heating on both the gas fraction and temperature of the clusters. Cooling removes low-entropy (core) gas from the halo, causing higher-entropy material to flow in to replace it. This results in a lower gas fraction, although the remaining gas is hotter (Pearce et al. 2000; Bryan 2000; Muanwong et al. 2001). For low-mass clusters ($M_{200} < 10^{14}\ h^{-1}\ {\rm M}_\odot$), the net effect of cooling on Y is dominated by the decrease in hot gas fraction, shown in Fig. 2, around a factor of 2 lower than the *Non-radiative* average at $M_{200} = 10^{13}\ h^{-1}\ {\rm M}_\odot$. For the highest-mass clusters, this difference decreases to around 30 per cent; combined with the increase in temperature of the gas, the clusters have very similar Y values in the two simulations.

In the *Preheating* case, the energy injection at high redshift heats the gas and expels some of it from the cluster. Hence its effect on the cluster properties is similar to the cooling model, but the fate of the gas is different (Muanwong et al. 2002). Fig. 2 shows that the gas fraction in *Preheating* clusters increases more rapidly with mass than for objects in the *Cooling* simulation [the reader should refer to section 3.1 and fig. 3 of Muanwong et al. (2002) for a detailed discussion of the hot, cold and total baryonic mass fractions in clusters for the same set of simulations]. In low-mass systems, the heating energy was sufficient to decrease $f_{\rm gas}$ (and hence Y) significantly, but left the gas fractions almost unchanged in the highest-mass clusters, where the heating resulted only in a modest increase in temperature. Note, therefore, that the best-fitting relation is only a good description of the low-mass clusters in the *Preheating* simulation; systems more massive than $\sim 10^{14}\ h^{-1}\ {\rm M}_\odot$ are adequately described by the *Non-radiative* relation. This also explains why White et al. (2002) find good agreement with the self-similar $Y_{\rm int}$–M scaling, as they only investigated high-mass clusters ($M_{200} \geqslant 5 \times 10^{14}\ h^{-1}\ {\rm M}_\odot$), where a high fraction of the wind material would have been retained.

The effects of cooling and preheating on the cluster properties are more readily apparent in the relation between Y and mass-weighted temperature. For a cluster of fixed gas and total mass, $Y \propto T_{\rm mw}$, and so heating the gas causes a shift to the right of the steeper self-similar relation ($Y \propto T^{5/2}$). Additionally, the decrease in gas

fraction lowers Y, separating the two relations further. The best-fitting $Y^{\rm int}_{200}$–$T_{\rm mw}$ relations are as follows:
Non-radiative run:

$$Y^{\rm int}_{200} = 5.59 \times 10^{-7} \left(\frac{k_{\rm B}T_{\rm mw}}{1\,{\rm keV}}\right)^{2.63} (h^{-1}\,{\rm Mpc})^2, \quad (14)$$

Cooling run:

$$Y^{\rm int}_{200} = 2.51 \times 10^{-7} \left(\frac{k_{\rm B}T_{\rm mw}}{1\,{\rm keV}}\right)^{2.90} (h^{-1}\,{\rm Mpc})^2, \quad (15)$$

Preheating run:

$$Y^{\rm int}_{200} = 2.23 \times 10^{-7} \left(\frac{k_{\rm B}T_{\rm mw}}{1\,{\rm keV}}\right)^{3.03} (h^{-1}\,{\rm Mpc})^2. \quad (16)$$

4.2 The Y–$T_{\rm X}$ relation

Of more practical interest is to investigate how Y correlates with X-ray observables, particularly luminosity and emission-weighted temperature.

Fig. 3 illustrates the relationship between $Y^{\rm int}_{200}$ and $T_{\rm X}$ for the *Cooling* (top panel) and *Preheating* (bottom panel) simulations. Circles represent clusters for which all hot gas particles within R_{200} are considered, whereas crosses are for the same clusters but excluding particles within the cooling radius in the computation of the temperature. We define the cooling radius as the radius within which the gas has a mean cooling time of 6 Gyr. (This procedure is an attempt to provide a 'cooling flow' correction to the estimated values of $T_{\rm X}$.)

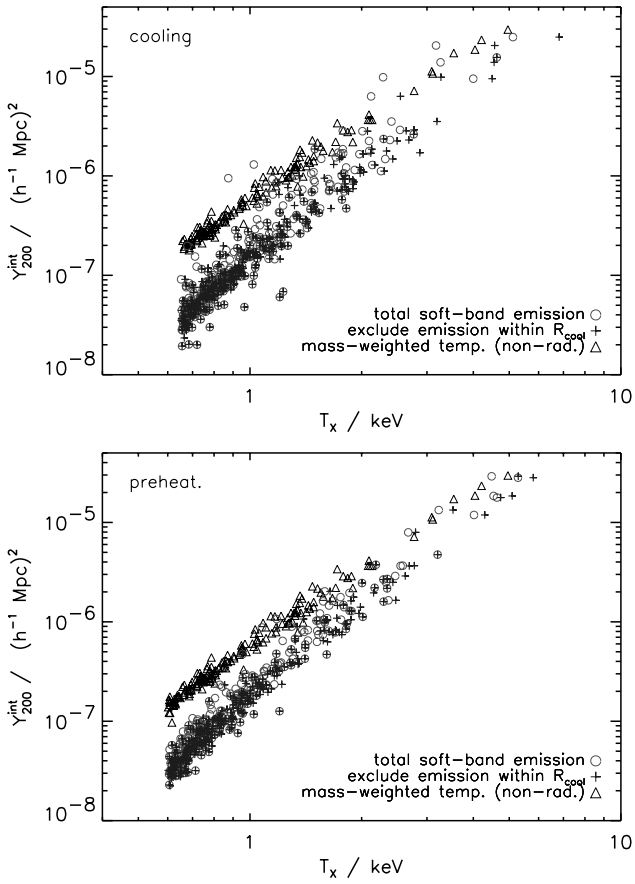

Figure 3. $Y^{\rm int}_{200}$ versus $T_{\rm X}$ for clusters in the *Cooling* (top panel) and *Preheating* (bottom panel) simulations, including (circles) and excluding (crosses) soft-band emission from within the cooling radius. Also shown for comparison is the scaling with the mass-weighted temperature found in the *Non-radiative* simulation (triangles).

Table 1. Power-law fits to the simulated cluster Y–$T_{\rm X}$ and Y–$L_{\rm X}$ scalings at $z = 0$. Here α_T and α_L are the slopes of the $Y^{\rm int}_{200}$–$T_{\rm X}$ and $Y^{\rm int}_{200}$–$L_{\rm X}$ relations, whereas $A_T/10^7$ and $A_L/10^7$ are the values of $Y^{\rm int}_{200}$ derived from these relations at $k_{\rm B}T_{\rm X} = 1$ keV and $L_{\rm X} = 10^{43}\ h^{-2}$ erg s^{-1}, respectively.

	$Y^{\rm int}$–$T_{\rm X}$		$Y^{\rm int}$–$L_{\rm X}$	
Run	α_T	A_T	α_L	A_L
Non-radiative (bolometric)	2.47	10.1	1.26	0.37
Cooling (soft band)				
uncorrected	3.35	1.64	0.94	4.72
cooling-flow-corrected	3.06	1.41	1.09	6.51
Preheating (soft band)				
uncorrected	3.26	1.93	0.98	6.65
cooling-flow-corrected	3.18	1.70	1.04	8.09

Comparing these results with Fig. 1, we see that the scatter is larger for the correlation with $T_{\rm X}$ than with $T_{\rm mw}$. This is because $T_{\rm X}$ is weighted by density and temperature and is therefore more sensitive to substructure, particularly from the centres of clusters. This is also evident from the fact that the scatter is smaller when the gas within the cooling radius is excluded (note that this also increases $T_{\rm X}$ in high-mass systems, which slightly flattens the Y–$T_{\rm X}$ relation).

Table 1 lists best-fitting coefficients, α_T and A_T, to the power law $Y^{\rm int}_{200} = (A_T/10^7)(k_{\rm B}T_{\rm X}/1\,{\rm keV})^{\alpha_T}$ for the *Cooling* and *Preheating* runs. (We also present results from the *Non-Radiative* run, using a bolometric cooling function, and this agrees well with the self-similar scaling $Y \propto T^{5/2}$.) For a given run, the normalization of the $Y^{\rm int}_{200}$–$T_{\rm X}$ relation is lower and the slope is steeper than for the $Y^{\rm int}_{200-T{\rm mw}}$ relation. The heavier weighting of the denser gas exacerbates the effects of cooling/heating on the Y–T relation discussed in the previous section.

4.3 The Y–$L_{\rm X}$ relation

We end this section by reporting on the $z = 0$ correlation between $Y^{\rm int}$ and bolometric X-ray luminosity $L_{\rm X}$, as inferred from the soft-band emission. Fig. 4 shows the $Y^{\rm int}_{200}$–$L_{\rm X}$ relation from the *Cooling* (top panel) and *Preheating* (bottom panel) simulations. Again, we use circles to represent values including all hot gas particles, whereas crosses represent results when excluding gas from within the cooling radius. The best-fitting parameters α_L and A_L, defined by $Y^{\rm int}_{200} = (A_L/10^7)(L_{\rm X}/L_{43})^{\alpha_L}$, where $L_{43} = 10^{43}\ h^{-2}$ erg s^{-1}, are listed in Table 1.

The *Cooling* and *Preheating* relations are significantly shallower than the predicted self-similar scaling, $Y \propto L^{5/4}$, which is well reproduced by the *Non-radiative* simulation (where $\alpha_L = 1.26$). Again, this is due to the increase in entropy of the gas, particularly in low-mass clusters, which decreases their luminosity. Omitting gas from within the cooling radius slightly increases the slope of the $Y^{\rm int}$–$L_{\rm X}$ relation and also reduces the scatter.

5 EVOLUTION OF SCALING RELATIONS

We now investigate the evolution of the scaling relations with redshift. In each of the following subsections, we factor out the dependence expected from self-similar evolution. Note that the self-similar evolution has no dependence on Ω_0 because we define the overdensity with respect to the comoving critical density.

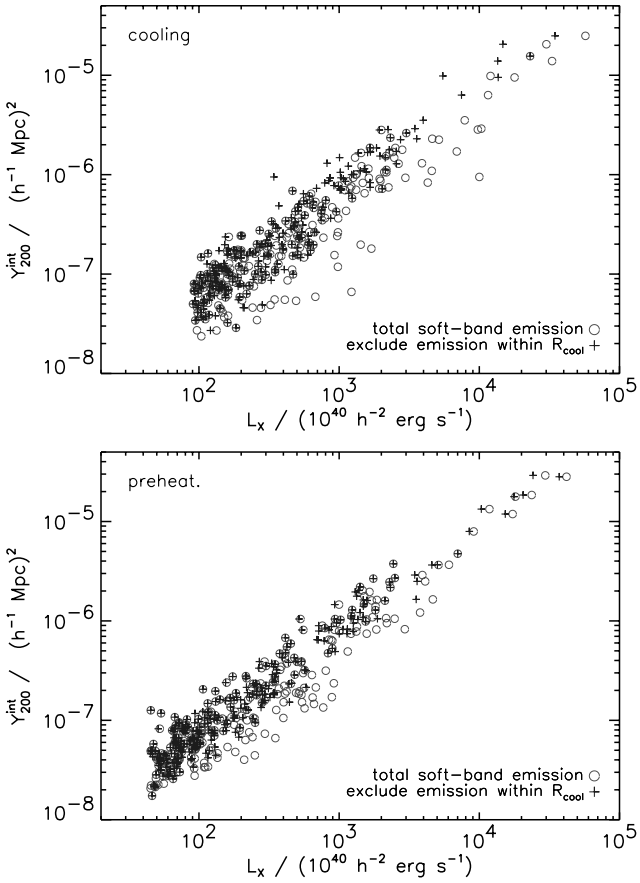

Figure 4. $Y^{\rm int}_{200}$ versus $L_{\rm X}$ for clusters at $z = 0$ in the *Cooling* (top panel) and *Preheating* (bottom panel) simulations. Circles (crosses) denote objects when gas within the cooling radius is included (excluded) in the calculations.

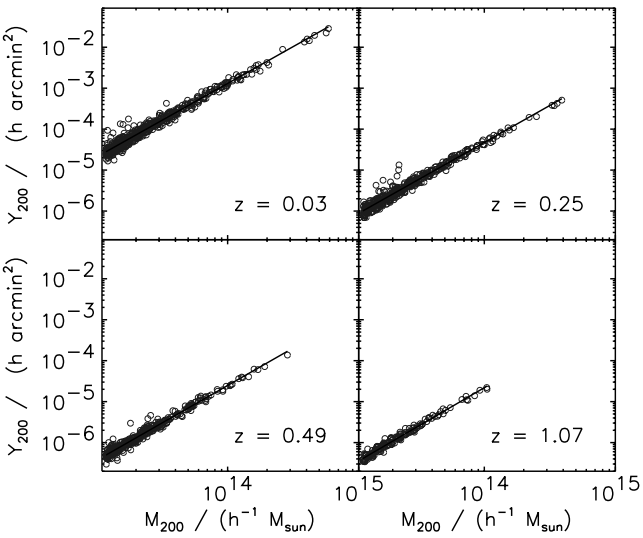

Figure 5. Y_{200}–M_{200} relation at various redshifts for the *Cooling* simulation. The solid line is the power-law best fit.

5.1 Evolution of the *Y*–*M* relation

Fig. 5 shows the Y_{200}–M_{200} relation for clusters in the *Cooling* simulations, for a range of redshifts between $z \sim 0$ and $z \sim 1$. Here we use $Y_{200} = Y^{\rm int}_{200} d_{\rm A}^{-2}$, demonstrating the dominant effect of $d_{\rm A}$ on Y at these redshifts. Note that the number of clusters satisfying our mass selection criteria, $M_{200} \gtrsim 1.18 \times 10^{13}\ h^{-1}\ {\rm M}_\odot$, decreases with increasing redshift.

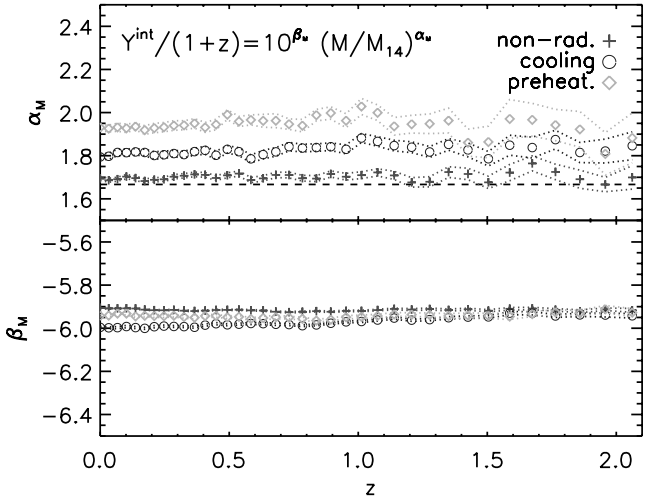

Figure 6. Redshift dependence of the slope (α_M) and normalization (β_M) of the cluster $Y^{\rm int}_{200}$–M_{200} relation in the *Non-radiative* (crosses), *Cooling* (circles) and *Preheating* (diamonds) simulations. Symbols represent best-fitting parameters and the dotted lines are their 1σ uncertainties (see text). The dashed line represents the slope predicted by the self-similar model ($\alpha_M = 5/3$).

A noticeable feature of Fig. 5 is the apparent independence of the slope of the Y_{200}–M_{200} relation with redshift. To quantify the effects of cooling and heating on the evolution of the slope, we fit a power law,

$$\frac{Y^{\rm int}_{200}}{1+z} = 10^{\beta_M(z)} \left(\frac{M_{200}}{10^{14}\ h^{-1}\ {\rm M}_\odot} \right)^{\alpha_M(z)}, \tag{17}$$

to the distribution of clusters at each redshift, and plot the resulting best-fitting values of α_M against z in the upper panel of Fig. 6. (We do not plot results for redshifts beyond 2, as the number of clusters below our mass threshold becomes too small for a reliable fit to be produced.) Crosses, circles and diamonds represent best-fitting values, and dotted lines denote 1σ uncertainties (estimated using the method given by Press et al. 1992) from the *Non-radiative, Cooling* and *Preheating* simulations respectively. Indeed, the results are consistent with an unevolving slope for all three models out to $z = 2$.

The lower panel of Fig. 6 shows the evolution of the normalization, obtained by fitting the same power-law function as before, but with a fixed slope taken to be equal to the mean value of $\alpha_M(z)$ within the displayed range of z (values are given in Table 2). From this figure, we see that the evolution of the $Y^{\rm int}_{200}$–M_{200} normalization is remarkably self-similar for all runs. Fitting a power law, $10^{\beta_M(z)} \propto (1+z)^{\gamma_M}$, to the derived normalizations (within the displayed range of z), we find that the largest deviation from self-similar evolution of the normalization is only $\gamma_M = 0.14$, for the *Cooling* simulation (Table 2).

It is therefore clear that the evolution of the $Y_{\rm int}$–M_{200} relation is not a sensitive probe of underlying non-gravitational physics, as it is a measure of the large-scale evolution of clusters. As discussed in McCarthy et al. (2003a), the effects of cooling and preheating are much more apparent if the SZ flux density is evaluated within a smaller radius, where the average gas density is higher. As we shall

Table 2. Deviations from self-similarity in the mean slope and normalization of the SZ scaling relations. The quantities $\langle\alpha_M\rangle$, $\langle\alpha_T\rangle$ and $\langle\alpha_L\rangle$ are the mean values of the best-fitting slopes of the $Y_{200}^{\rm int}$–M_{200}, $Y_{200}^{\rm int}$–$T_{\rm X}$ and $Y_{200}^{\rm int}$–$L_{\rm X}$ relations, respectively, averaged over redshifts $z = 0$ to 2. The quantities γ_M, γ_T and γ_L are power-law best fits to the normalization of the scalings, $10^{\beta(z)} \propto (1+z)^{\gamma}$; the first two are a good fit for the complete redshift range, but for luminosity the fit is restricted to $0 < z < 1$.

	Mean slope deviation from self-similarity		
Run	$\langle\alpha_M\rangle - 5/3$	$\langle\alpha_T\rangle - 5/2$	$\langle\alpha_L\rangle - 5/4$
Cooling	0.16	0.44	−0.16
Preheating	0.28	0.52	−0.22
	Normalization deviation from self-similarity		
Run	γ_M	γ_T	γ_L
Cooling	0.14	0.73	1.30
Preheating	0.02	0.33	1.62

see, such effects are apparent when studying the evolution of the X-ray properties of the clusters.

5.2 Evolution of the Y–$T_{\rm X}$ relation

Fig. 7 shows the redshift dependence of the slope and normalization of the Y–$T_{\rm X}$ relation for the *Cooling* and *Preheating* simulations, using cooling-flow-corrected temperatures. As in the previous section, we first fit the cluster distribution at each redshift with a power law,

$$\frac{Y_{200}^{\rm int}}{(1+z)^{-3/2}} = 10^{\beta_T(z)} \left(\frac{T_{\rm X}}{\rm keV}\right)^{\alpha_T(z)}, \tag{18}$$

to determine the evolution of the slope. While this shows significant statistical oscillations (reflecting the higher sensitivity of the emission-weighted temperature to the thermal history of the gas), there is no evidence of evolution with redshift beyond that predicted by self-similarity. The slope is then fixed at the mean value, $\langle\alpha_T\rangle$, before determining the redshift dependence of the normalization, $\beta_T(z)$. Unlike the $Y^{\rm int}$–M relation, there is a definite evolutionary trend that is particularly significant in the *Cooling* case. This is an

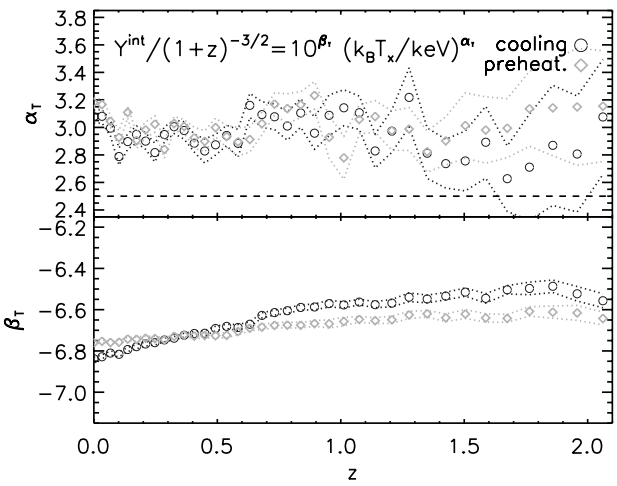

Figure 7. Redshift dependence of the slope (α_T) and normalization (β_T) of the cluster $Y_{200}^{\rm int}$–$T_{\rm X}$ relation in the *Cooling* (circles) and *Preheating* (diamonds) simulations. Symbols represent best-fitting values and dotted lines their 1σ uncertainties. The dashed line represents the slope predicted by the self-similar model ($\alpha_T = 5/2$).

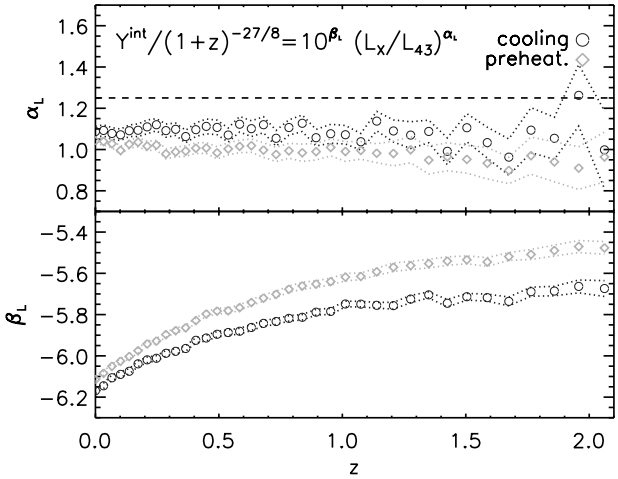

Figure 8. Redshift dependence of the slope (α_L) and normalization (β_L) of the cluster $Y_{200}^{\rm int}$–$L_{\rm X}$ relation in the *Cooling* (circles) and *Preheating* (diamonds) simulations. Symbols represent best-fitting parameters and dotted lines their 1σ uncertainties. The dashed line represents the slope predicted by the self-similar model ($\alpha_L = 5/4$).

indication that evolution is predominantly in the X-ray properties rather than in the SZ signal, which is much less sensitive to the details of the gas distribution in the central regions of clusters. Fitting the normalizations with a power law of the form $10^{\beta_T(z)} \propto (1+z)^{\gamma_T}$, we find $\gamma_T = 0.73$ and 0.33 for the *Cooling* and *Preheating* simulations, respectively. In both cases the normalization of the $T_{\rm X}$–M relation increases with time compared to the expected self-similar evolution.

5.3 Evolution of the Y–$L_{\rm X}$ relation

We end by studying the evolution of the Y–$L_{\rm X}$ relation, shown in Fig. 8. Our power-law fitting function was

$$\frac{Y_{200}^{\rm int}}{(1+z)^{-27/8}} = 10^{\beta_L(z)} \left(\frac{L_{\rm X}}{L_{43}}\right)^{\alpha_L(z)}, \tag{19}$$

using cooling-flow-corrected values for $L_{\rm X}$. Again, the slopes are constant with redshift to good approximation, and there is additional evolution in the normalization. In this case a single power law is not such a good fit over the complete redshift range, and we restrict the fit to $0 < z < 1$, which is where observations are likely to be made. Fitting a power law $10^{\beta_L(z)} \propto (1+z)^{\gamma_L}$ yields $\gamma_L \sim 1.3$ and 1.6 in the *Cooling* and *Preheating* cases respectively (Table 2) in this redshift range, with the relation flattening at redshifts beyond unity.

6 CONCLUSIONS

In this paper, we investigated the relationship between SZ and X-ray properties of clusters drawn from three simulations: a *Non-radiative* simulation, where the gas could only heat adiabatically and through shocks; a *Cooling* simulation, where the gas could also cool radiatively; and a *Preheating* simulation, where we additionally heated the gas by 1.5 keV per particle at $z = 4$. We focused on the relations between the thermal SZ signal $Y_{\rm int}$ and cluster mass, temperature and X-ray luminosity, both at $z = 0$ and the evolution with redshift. Our main conclusions are as follows:

(i) $Y_{\rm int}$ is tightly correlated with both mass and mass-weighted temperature. Scaling relations of $Y_{\rm int}$ with X-ray quantities show

significantly more scatter, however, due to the sensitivity of the latter (which are emission-weighted) to the gas distribution in the cores of clusters. Excluding gas from within the cooling radius of each cluster reduces the scatter.

(ii) The *Non-radiative* simulation scaling relations closely match those predicted by the self-similar model, with $Y_{\rm int} \propto T_{\rm X}^{5/2}$ and $Y_{\rm int} \propto L_{\rm X}^{5/4}$.

(iii) *Cooling* decreases $Y_{\rm int}$ for a given cluster mass, due to the reduction in the hot gas fraction (which decreases $Y_{\rm int}$) being more effective than the increase in temperature of the remaining gas (which increases $Y_{\rm int}$). *Preheating* the gas has a similar effect except in the most massive clusters, where the heating energy was not sufficient to expel much gas from the halo. At zero redshift, the resulting $Y_{\rm int}$–$T_{\rm X}$ scaling relation is steeper than the self-similar relation, $Y_{\rm int} \propto T_{\rm X}^{3.0-3.4}$, and the $Y_{\rm int}$–$L_{\rm X}$ relation is flatter, $Y_{\rm int} \propto L_{\rm X}^{0.9-1.1}$.

(iv) There is no evidence of evolution in the slopes of any of the scaling relations. The normalization of the Y_{200}–M_{200} relation is also consistent with self-similar evolution. However, the relations between $Y_{\rm int}$ and the cluster X-ray properties do show significant evolution in normalization relative to that expected from self-similarity, indicating that evolution is predominantly in the X-ray properties rather than the SZ properties. The effects of excess entropy reduce the negative evolution of the $Y_{\rm int}$–$T_{\rm X}$ and $Y_{\rm int}$–$L_{\rm X}$ with redshift, particularly at $z < 1$.

ACKNOWLEDGMENTS

ACdS was supported by the EU CMBNET network, STK by PPARC, and ARL in part by the Leverhulme Trust. The simulations used in this paper were carried out on the Cray-T3E (RIP) at the EPCC as part of the Virgo Consortium programme of investigations into the formation of structure in the Universe. ACdS acknowledges the use of the computer facilities at CALMIP-CICT, France, and visits to Sussex supported by PPARC.

REFERENCES

Bower R. G., 1997, MNRAS, 288, 355
Bower R. G., Benson A. J., Lacey C. G., Baugh C. M., Cole S., Frenk C. S., 2001, MNRAS, 325, 497
Bryan G. L., 2000, ApJ, 544, L1
Cavaliere A., Menci N., 2001, MNRAS, 327, 488
Cole S. et al. (the 2dFGRS team), 2001, MNRAS, 326, 255
Couchman H. M. P., Thomas P. A., Pearce F. R., 1995, ApJ, 452, 797
da Silva A. C., Kay S. T., Liddle A. R., Thomas P. A., Pearce F. R., Barbosa D., 2001, ApJ, 561, L15
Edge A. C., Stewart G. C., 1991, MNRAS, 252, 414
Eke V. R., Navarro J. F., Frenk C. S., 1998, ApJ, 503, 569
Evrard A. E., Henry J. P., 1991, ApJ, 383, 95
Holder G. P., Carlstrom J. E., 2001, ApJ, 588, 515
Kaiser N., 1986, MNRAS, 222, 323
Kaiser N., 1991, ApJ, 383, 104
Knight P. A., Ponman T. J., 1997, MNRAS, 289, 955
McCarthy I. G., Babul A., Holder G. P., Balogh M. L., 2003a, ApJ, 591, 515
McCarthy I. G., Holder G. P., Babul A., Balogh M. L., 2003b, ApJ, 591, 526
Mather J. C., Fixsen, D. J., Shafer R. A., Mosier C., Wilkinson D. T., 1999, ApJ, 512, 511
Metzler C. A., 1998, astro-ph/9812295
Muanwong O., Thomas P. A., Kay S. T., Pearce F. R., Couchman H. M. P., 2001, MNRAS, 552, L27
Muanwong O., Thomas P. A., Kay S. T., Pearce F. R., 2002, MNRAS, 336, 527
Navarro J. F., Frenk C. S., White S. D. M., 1995, MNRAS, 275, 720
Navarro J. F., Frenk C. S., White S. D. M., 1997, ApJ, 490, 493
Pearce F. R., Couchman H. M. P., 1997, New Astron., 2, 411
Pearce F. R., Thomas P. A., Couchman H. M. P., Edge A. C., 2000, MNRAS, 317, 1029
Ponman T. J., Sanderson A. J. R., Finoguenov A., 2003, MNRAS, 343, 331
Press W. H., Teukolsky S. A., Vetterling W. T., Flannery B. P., 1992, Numerical Recipes in Fortran. Cambridge Univ. Press, Cambridge
Quilis V., Bower R. G., Balogh M. L., 2001, MNRAS, 328, 1091
Raymond J. C., Smith B. W., 1977, ApJS, 35, 419
Springel V., Hernquist L., 2003, MNRAS, 339, 312
Springel V., White M., Hernquist L., 2001, ApJ, 549, 681
Sunyaev R. A., Zel'dovich Ya. B., 1972, Comments Astrophys. Space Phys., 4, 173
Sunyaev R. A., Zel'dovich Ya. B., 1980, ARA&A, 18, 537
Sutherland R. S., Dopita M. A., 1993, ApJS, 88, 253
Thacker R. J., Couchman H. M. P., 2000, ApJ, 545, 728
Thomas P. A., Couchman H. M. P., 1992, MNRAS, 257, 11
Thomas P. A. et al. (the Virgo Consortium), 1998, MNRAS, 296, 1061
Thomas P. A., Muanwong O., Kay S. T., Liddle, A. R., 2002, MNRAS, 330, L48
Voit G. M., Bryan G. L., Balogh M. L., Bower R. G., 2002, ApJ, 576, 601
White M., Hernquist L., Springel V., 2002, ApJ, 579, 16
Wu K. K. S., Fabian A. C., Nulsen P. E. J., 2000, MNRAS, 318, 889
Xue Y.-J., Wu X.-P., 2000, ApJ, 538, 65
Zhang Y.-Y., Wu X.-P., 2003, ApJ, 583, 529

This paper has been typeset from a TEX/LATEX file prepared by the author.